Atomic Spectroscopy

Article

Determining Mg Isotope Compositions of the Silicate Fraction of Detrital Sedimentary Rocks via Acid Leaching

Dongye Teng,[a] Beibei Chen,[b] Hongsheng Xu,[a] Yongsheng He,[a,*] Shouming Chen,[c,*] and Shan Ke [a]

[a] State Key Laboratory of Geological Processes and Mineral Resources, Frontiers Science Center for Deep-time Digital Earth, China University of Geosciences, Beijing 100083, P. R. China

[b] School of Earth Sciences and Resources, China University of Geosciences, Beijing 100083, P. R. China

[c] Institute of Geology, Chinese Academy of Geological Sciences, Beijing 100037, P. R. China

Received: *December 04, 2025;* ***Revised:*** *December 30, 2025;* ***Accepted:*** *January 24, 2026;* ***Available online:*** *January 24, 2026.*

DOI: 10.46770/AS.2025.284

ABSTRACT: Magnesium (Mg) isotopic composition of sedimentary silicate fractions provides key critical constraints on the history of silicate weathering and climate evolution. Since sedimentary rocks typically contain authigenic carbonates, standard whole-rock digestion co-dissolves both carbonate and silicate phases, resulting in hybridized Mg isotope signals. Accurate analysis therefore requires separation of silicate components through selective dissolution methods that exclude Mg from carbonates. However, standardized dissolution methods specifically designed for Mg isotope analysis of the silicate phase in sedimentary rocks are still lacking. Significant variations exist among different pretreatment protocols, particularly in the choice of leaching reagents and cleaning procedures. And the Mg isotope fractionation behavior of silicate phases under different acid reagents and leaching procedures remains unclear. In particular, the effects of strong acids on silicate components and the potential extent of induced fractionation are not well constrained. This issue becomes notably critical in studies requiring high-precision Mg isotope analysis. In this investigation, we have systematically designed and performed chemical leaching experiments on Marinoan diamictites from South China to develop an optimized and robust leaching pretreatment scheme for Mg isotope studies of clastic silicate fractions. Our results demonstrate that 0.5 mol·L^{-1} Acetic acid (HAc) exhibits limited efficiency in leaching poorly soluble carbonate minerals (*e.g.*, siderite), as shown by only 7.7% and 1.4% decreases in the leached residue's Mg/Al and Fe/Al ratios relative to the whole-rock values. For samples containing Mg-rich and Fe-rich carbonates, 0.4 mol·L^{-1} hydrochloric acid (HCl) is recommended to ensure efficient carbonate removal and subsequent reliable acquisition of silicate Mg isotope signatures. This study provides the essential experimental basis for developing sedimentary Mg isotopes as a quantitative paleoenvironmental proxy, thereby enabling more refined reconstructions of Earth's surface evolution.

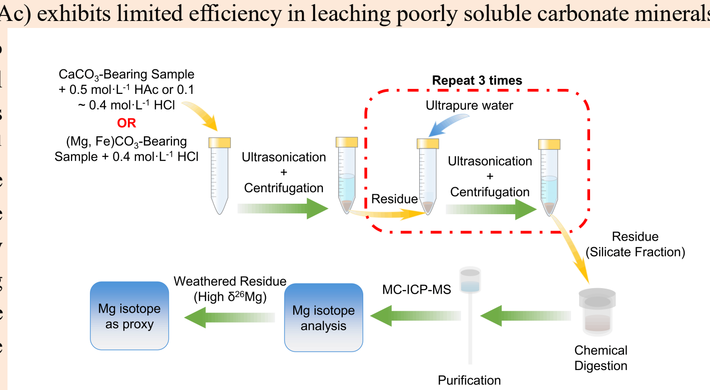

INTRODUCTION

Continental weathering is a fundamental geological process that couples the atmosphere, hydrosphere, and lithosphere, playing a key role in regulating the global carbon cycle and climate. [1-5] The study of chemical weathering extends beyond decoding past climate evolution to include providing an essential basis for understanding and projecting future climate system behavior. Chemical weathering and associated surface processes transform the mineralogical and geochemical characteristics of freshly exposed bedrock, encoding weathering information within the altered compositions. These products are ultimately preserved as sedimentary rocks and detrital sediments, forming a crucial archive for reconstructing silicate weathering history in source regions. [6-8] Various geochemical proxies in sedimentary records, such as Chemical Index of Alteration (CIA), strontium (Sr), lithium (Li), and magnesium (Mg) isotopes, have been proposed to effectively trace continental chemical weathering. [9-12]

Magnesium, is a water-soluble major element in the crust that is systematically mobilized and isotopically fractionated during weathering.[13,14] This fractionation is characterized by the preferential release of light Mg isotopes into the fluid phase, while heavy isotopes are retained and enriched in the residual solid, producing Mg isotopic variations of up to 2‰ in weathering systems. [14-16] Moreover, the Mg isotopic system in siliciclastic rocks is resistant to low-grade metamorphic alteration, suggesting that the Mg isotopic compositions of the silicate fraction can reliably retain and reveal source characteristics. [17] Therefore, Mg isotopes have been increasingly applied as proxies for chemical weathering processes. [18-20] However, the presence of Mg hosted in primary carbonates in sedimentary rocks may compromise the Mg isotopic signature of detrital silicate fractions that record continental weathering signals. Acid leaching methods are routinely employed to selectively remove carbonate components from geological samples such as carbonate rocks, glacial diamictites, and clastic sedimentary rocks. [15, 18-20] However, the carbonate leach is unlikely to have been totally efficient, since any attempt to fully dissolve carbonates will inevitably lead to the premature alteration of other phases, such as silicates. [21] Within current analytical workflow for silicate-phase Mg isotope analysis, the effectiveness of leaching methods used to remove carbonate components from bulk sedimentary rocks has not been systematically investigated. Although a range of leaching protocols have been employed in previous studies, including stepwise leaching using 0.5 $mol \cdot L^{-1}$ acetic acid (HAc) with 0.5 $mol \cdot L^{-1}$ hydrochloric acid (HCl), 0.5 $mol \cdot L^{-1}$ HAc with 1 $mol \cdot L^{-1}$ HCl, and direct leaching with 3 $mol \cdot L^{-1}$ HCl, [15, 18-20] their impact on silicate-phase Mg isotopic compositions remains insufficiently constrained. The uncertainty is particularly pronounced for glacial diamictites, which are sedimentary rocks formed under extreme icehouse conditions. This is because siderite insoluble in weak acids has been identified in glacial-marine sedimentary records from the Marinoan deglaciation period. [22] When performing acid leaching on such samples, the use of weak acids may lead to incomplete dissolution of insoluble carbonate. Residual carbonates containing Mg can then interfere with the analysis of continental weathering signals. Conversely, the use of strong acids may cause excessive dissolution, attacking silicate components and potentially inducing artificial fractionation of Mg isotopes in the silicate phases. Currently, the optimal approach in practice involves maximizing the dissolution and removal of carbonate components to prevent contamination of the weathering signal carried by Mg isotopes from primary carbonates, while simultaneously minimizing artificial fractionation effects induced by silicate dissolution. However, a systematic evaluation of different leaching methods is lacking. This makes it difficult to determine to what extent the final isotopic composition is influenced by Mg contamination from incompletely removed carbonates during acid leaching, or whether isotope fractionation occurs during the leaching process due to partial dissolution of silicate phases.

In this study, a series of chemical leaching experiments was performed on Marinoan diamictites from South China, with the purpose of investigating the effects of key variables such as reagent type and concentration. Combined with elemental and mineralogical data, an optimized single-step chemical pretreatment protocol was established for the accurate analysis of Mg isotopes in silicate fractions of these diamictites. Through comparative evaluation, a leaching method was recommended that effectively removes complex carbonate phases, including Mg- and Fe-rich carbonates, while preserving the primary Mg isotope signals of the silicate fractions.

EXPERIMENTAL

Samples. Cryogenian glacial deposits are widely distributed in the Yangtze Block. The Nantuo Formation is the younger glacial deposit of Cryogenian stratigraphic succession and is equivalent to Marinoan glaciation (approximately 639 – 635 Ma). [23-25] It mainly consists of massive diamictite and crudely stratified diamictite. In this study, six Nantuo Formation diamictite samples from a 71.4-m-thick interval (drill core ZK101; Changyang County, Hubei Province) were utilized to optimize leaching protocols to extract silicate fractions for Mg isotope analysis. Spatial heterogeneity of pebbles and coarse-grained clasts in diamictites can cause sampling bias, leading to skewed bulk composition measurements. The matrix of glacial diamicton is thus interpreted as a more reliable recorder of weathering intensity variations in provenance terrains. [15, 26, 27] Accordingly, diamictite samples were crushed to particles approximately 3 - 5 mm in diameter, and the matrix materials were visually isolated and further pulverized to 200-mesh powder for subsequent leaching experiments.

Typical glacial diamictites are primarily composed of a silty and clayey matrix containing gravels of diverse compositions, with the gravels being poorly sorted and ranging from angular to rounded in outline. [28] Six glacial diamictite samples from the studied section were carefully selected to cover heterogeneity in lithological assemblage of the Nantuo Formation. The matrix of the glacial diamictite examined in this study consists of clay- to silt-sized detrital materials, predominantly composed of quartz, clay minerals (illite and clinochlore), albite, and carbonate minerals. Detailed major element concentrations and mineral proportions are provided in Supplementary Data (Tables S1 and S2). The six selected representative samples contain 1% – 10% carbonate minerals, which include both calcic carbonates (calcite) and Fe-Mg-rich carbonate varieties (*e.g.*, siderite).

Table 1. Design for the leaching experiments of diamictites to remove carbonate components

No.	Experimental Group	Reagents	Sample Mass/mg	Reagent Volume/mL
1	untreated control	/	~ 4 – 8	/
2	weak acid	0.5 mol·L^{-1} HAc	~ 30	~ 10
3	low-concentration strong acid	0.1 mol·L^{-1} HCl	~ 30	~ 10
4	high-concentration strong acid	0.4 mol·L^{-1} HCl	~ 30	~ 10

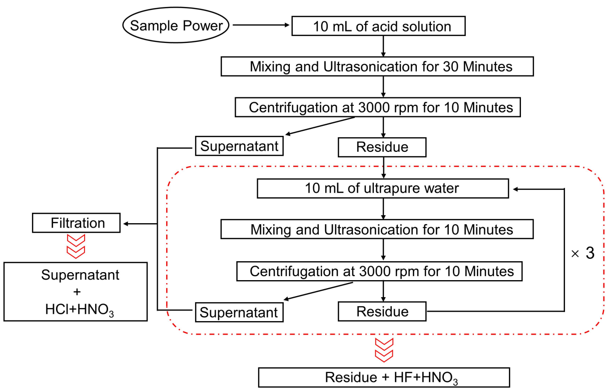

Fig. 1 Schematic diagram of the leaching experimental process.

Leaching Methods. HCl was selected as the leaching agent because it is a non-oxidizing strong acid, unlike nitric acid (HNO_3) or aqua regia, which could oxidize or alter oxidation-sensitive minerals. An additional advantage is that it reacts with carbonates to produce only soluble chlorides, water, and CO_2. HAc was employed as the weak acid reagent in this study. The one-step direct leaching approach was employed, and a series of four experiments was devised as follows: (1) untreated control, (2) weak acid leaching (0.5 mol·L^{-1} HAc), (3) low-concentration strong acid leaching (0.1 mol·L^{-1} HCl), and (4) high-concentration strong acid leaching (0.4 mol·L^{-1} HCl), as detailed in Table 1.

The leaching experiments and all elemental and isotopic analyses were conducted in the Isotope Geochemistry Laboratory at China University of Geosciences (Beijing). The leaching protocol was designed based on previous sequential extraction and carbonate-phase leaching methods, taking into account the specific lithological characteristics of the glacial diamictite.[29-31] Based on the stoichiometric ratio (2 mol HAc/HCl: 1 mol carbonate) and the carbonate content and mass of the samples, the theoretical volume of leaching acid required for complete reaction was estimated. The results showed that the needed acid volume was less than 1 mL for all samples in this study (Table S3). Therefore, to establish a uniform methodology, a constant excess volume of 10 mL of acid was employed in all experiments. The operational procedure is illustrated in Fig. 1 and described in detail below. Following the protocols outlined in Table 1 regarding reagent type, about 30 mg of sample powder was weighed into a 15 mL centrifuge tube. 10 mL of leaching reagents were then added, and the resulting mixture was vortexed thoroughly to ensure homogeneity before undergoing ultrasonication for 30 minutes at room temperature. Following ultrasonication, the mixture was centrifuged at 3000 rpm for 10 min. The supernatant was then collected by pipetting, and the residue in the centrifuge tube was processed further. The leached residues were subsequently rinsed with 10 mL of ultrapure water (18.25 MΩ) to remove residual leaching reagents, thoroughly mixed, and subjected to an additional 10-minute ultrasonication. Finally, the samples were centrifuged again at 3000 rpm for 10 minutes, and the supernatant was collected. After repeating the above washing steps three times, the residues were transferred to a beaker and dried on a hot plate at 80 °C. The collected residues were then subjected to the subsequent digestion and purification procedures same for Mg isotope analysis of whole rock samples. The collected supernatant was filtered through a syringe filter (0.45 µm, BKMAM Biotechnology Co., Ltd.) to remove potential contamination from particles. Untreated samples (whole rock) were used as a control group.

Reagents. The leaching reagent of 0.5 mol·L^{-1} HAc was prepared by quantitative dilution of high-purity HAc (ACS grade, ≥ 99.7%; Shanghai Macklin Biochemical Technology Co., Ltd.). Solutions of 0.1 mol·L^{-1} and 0.4 mol·L^{-1} HCl were prepared from acid pre-purified via distillation using a DST-1000 acid purification system (Savillex). The unpurified HCl source was BV-III grade, with a concentration of 36.0 ± 1.0% HCl (Beijing Institute of Chemical Reagents Co., Ltd.).

Elemental and Mg isotope determination. Sample digestion and Mg purification procedures followed established methods.[32, 33] Briefly, the recovered residue and whole rock powders were dissolved in a mixture of concentrated hydrofluoric acid (HF) and HNO_3 (23 mol·L^{-1} and 16 mol·L^{-1}, respectively), and then refluxed with aqua regia (HCl: HNO_3 = 3:1 in v/v) and concentrated HNO_3 sequentially. Complete digestion was ensured by visual confirmation of residue absence, and the dissolved samples were then transferred into a 1 mol·L^{-1} HNO_3 medium prior to purification.

Aliquot of each dissolved residue/filtered leaching supernatant was dried, redissolved in 3% HNO_3 (v/v), and diluted to 5 mL for elemental analysis, using an Inductively Coupled Plasma-Optical Emission Spectrometry (ICP-OES, *Agilent 5800*). The accuracy and precision of the interested elemental ratios, e.g., Ca/Al, Mg/Al, Fe/Al, Al/Ca, Mg/Ca, and Fe/Ca, assessed using reference materials BHVO-2 and GSP-2, were better than 10%.

Aliquot of sample solutions containing ca. 20 µg of Mg were loaded on pre-cleaned columns (4 mm in diameter; 20.5 cm in length) filled with 2.3 mL AG50W-X8 resin (200 to 400 mesh

Table 2. Major element ratios of selected diamictites and their leachate-residue pairs derived from acid leaching experiments

Sample No.	Ca/Al	Mg/Al	Fe/Al	Al/Ca	Mg/Ca	Fe/Ca
	mol/mol	mol/mol	mol/mol	mol/mol	mol/mol	mol/mol
Whole Rocks						
110.60-2	0.14	0.27	0.40	7.3	2.0	2.9
125.15-2	0.17	0.18	0.25	5.8	1.1	1.4
131.70-2	0.13	0.19	0.26	7.9	1.5	2.1
164.90-2	0.57	0.25	0.31	1.8	0.45	0.55
167.20-2	0.12	0.19	0.32	8.7	1.7	2.8
178.35-2	0.12	0.20	0.21	8.5	1.7	1.8
Leachate						
0.5 mol·L^{-1} HAc						
110.60-2	3.3	1.3	1.3	0.30	0.37	0.40
125.15-2	1.7	0.36	0.27	0.58	0.21	0.16
131.70-2	2.0	0.36	0.25	0.50	0.18	0.13
164.90-2	9.3	0.59	0.39	0.11	0.063	0.042
167.20-2	3.6	0.41	0.30	0.28	0.11	0.085
178.35-2	2.4	0.40	0.29	0.41	0.16	0.12
0.1 mol·L^{-1} HCl						
110.60-2	2.6	2.3	3.6	0.39	0.91	1.4
125.15-2	1.2	0.33	0.35	0.83	0.27	0.29
131.70-2	1.4	0.33	0.34	0.71	0.24	0.24
164.90-2	6.1	0.50	0.49	0.16	0.082	0.081
167.20-2	2.5	0.36	0.43	0.40	0.14	0.17
178.35-2	1.8	0.38	0.39	0.56	0.22	0.22
0.4 mol·L^{-1} HCl						
110.60-2	2.2	2.7	4.3	0.44	1.2	1.9
125.15-2	1.1	0.35	0.41	0.94	0.33	0.39
131.70-2	1.2	0.35	0.39	0.81	0.29	0.32
164.90-2	4.9	0.51	0.57	0.21	0.10	0.12
167.20-2	2.1	0.37	0.52	0.48	0.18	0.25
178.35-2	1.5	0.40	0.45	0.65	0.26	0.30
Residue						
0.5 mol·L^{-1} HAc						
110.60-2	0.012	0.25	0.39	82	21	32
125.15-2	0.012	0.16	0.25	84	14	21
131.70-2	0.0090	0.18	0.27	112	20	31
164.90-2	0.015	0.24	0.32	67	16	22
167.20-2	0.0069	0.19	0.33	144	28	48
178.35-2	0.022	0.19	0.21	45	8.5	9.6
0.1 mol·L^{-1} HCl						
110.60-2	0.0035	0.16	0.23	289	47	66
125.15-2	0.0047	0.15	0.24	214	33	51
131.70-2	0.0043	0.18	0.27	234	41	63
164.90-2	0.0061	0.24	0.32	164	39	52
167.20-2	0.0037	0.19	0.33	270	52	90
178.35-2	0.020	0.19	0.20	49	9.1	10
0.4 mol·L^{-1} HCl						
110.60-2	0.0023	0.12	0.14	443	52	64
110.60-2*	0.0026	0.12	0.14	389	45	54
125.15-2	0.0047	0.15	0.22	214	32	48
131.70-2	0.0043	0.17	0.26	233	40	61
164.90-2	0.0054	0.23	0.29	184	42	53
167.20-2	0.0037	0.19	0.32	272	51	88
178.35-2	0.020	0.18	0.20	49	8.9	9.7

Note:
*: the experiment was performed with a reagent-to-solid ratio of approximately 10:15 (mL:mg). Unless otherwise specified, the standard procedure employs a ratio of approximately 10:30 (mL:mg), with exact sample weights provided in Table 3.

hydrogen form, Bio-Rad), and Mg was collected by the 24th to 38th ml 1 mol·L^{-1} HNO_3, with matrix elements either being eluted in the first 23 mL of 1 mol·L^{-1} HNO_3 or retaining on the resin. The same column chemistry was performed twice to ensure the purity of the collected Mg. The purified Mg was dried down and re-dissolved in 1 ml of 0.15 mol·L^{-1} HNO_3 for isotope analysis. The

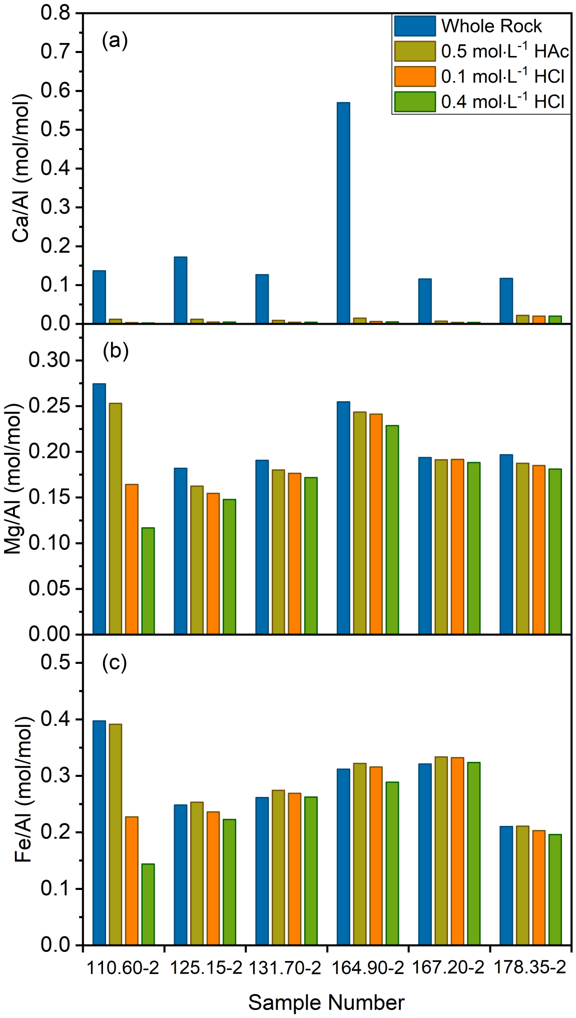

Fig. 2 Ca/Al, Mg/Al and Fe/Al ratios of whole rock and leached residues of the selected diamictites.

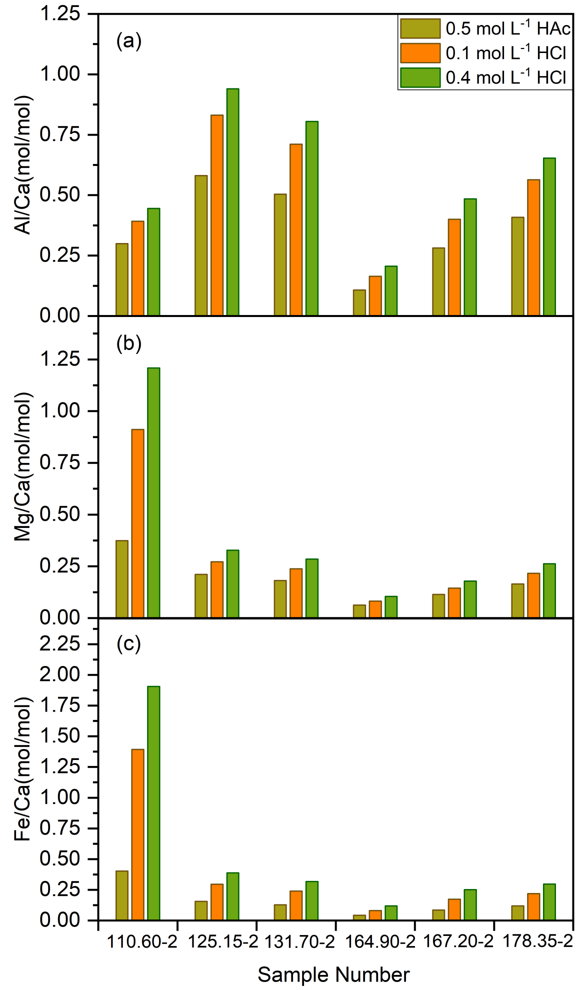

Fig. 3 Al/Ca, Mg/Ca, and Fe/Ca ratios in the leachates of the selected diamictites.

whole procedure blank was consistently below 5 ng, which is < 0.3‰ compared to the processed sample Mg and thus considered negligible.

Magnesium isotope analysis was conducted on a *Thermo Fisher Neptune Plus* MC-ICP-MS at low mass resolution mode, using the critical mixture double spike technique. [34] The sample solutions were spiked with a ^{25}Mg-^{26}Mg double spike (i.e., $^{25}Mg/^{24}Mg$ = 17.719, $^{26}Mg/^{24}Mg$ = 172.449) towards the optimized q value of 0.472 (q: the mole fraction of double spike in the mixture). The spiked samples were diluted to ~1 ppm in 0.15 mol·L^{-1} HNO_3 and introduced into the plasma via a PFA self-aspirating micro-nebulizer and a Scott-type double-pass quartz glass spray chamber. ^{24}Mg, ^{25}Mg, and ^{26}Mg were measured on the L3, C, and H3 Faraday cups, respectively, keeping the total ion signal intensity ≥ 50 V. Each measurement consisted of 80 cycles of 4.194 s integration each, and measurements of every five unknown samples were bracketed by those for spiked GSB Mg standard solutions. A set of over-/under-spiked GSB Mg standard solutions with q-values of 0.452, 0.462, 0.482, and 0.492 were measured in each analytical sequence to correct for the inaccuracy arising from the mismatching of the q of spiked samples with the optimized one (i.e., 0.472). The data were deduced offline and reported in the classic δ notion relative to DSM-3: $\delta^{26}Mg = [(^{26}Mg/^{24}Mg)_{sample}/(^{26}Mg/^{24}Mg)_{DSM\text{-}3} - 1] \times 1000$. [35] Each analytical sequence was typically measured four times; the mean values and two standard errors of the mean (2SE) are reported. Based on long-term monitoring on rocky and solution standards, the external precision (2SD) of $\delta^{26}Mg$ is ca. ± 0.03‰. Given the current lack of standardized procedures and certified reference values for leaching experiments, we assessed the accuracy and precision of the sample digestion, purification, and measurement protocols by analyzing the whole-rock Mg isotope composition of standard reference materials BHVO-2 and GSP-2. The rocky standards processed during the course of this study yield $\delta^{26}Mg$ values consistent with the reported values in the quoted errors (Table S4).[13, 34, 36] Furthermore, previous Mg isotopic analyses of carbonate and sedimentary rock reference materials conducted in our laboratory confirm that the existing chemical separation and analytical methods are broadly applicable to the glacial diamictite matrix examined in this study. [37]

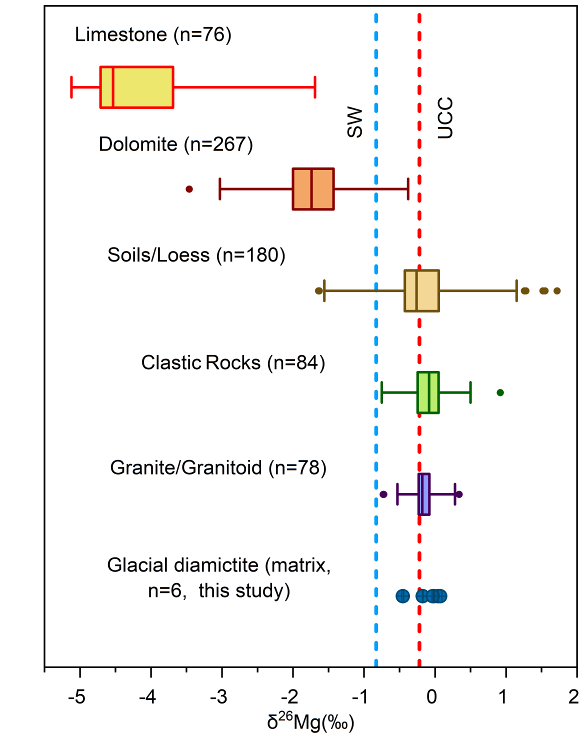

Fig. 4 This figure displays the $\delta^{26}Mg$ values of major magnesium reservoirs in crustal rocks, modified from the compiled dataset of Huang, et al. [15] and associated references. The box encompasses the 25 and 75 percentiles, the vertical line inside the box represents the median values, the whiskers represent the 2.5 and 97.5 percentiles, and the dots are outliers. The blue and red dashed lines indicate the Mg isotope values of seawater (-0.83‰) [48] and the upper continental crust (-0.22‰), [38] respectively. The Mg isotope values for the six glacial diamictites in this work are shown by the blue circles. Additional detailed data and corresponding literature references are provided in the Supplementary Table 5.

RESULTS AND DISCUSSION

Element and magnesium isotope compositions. The diamictites from South China show Ca/Al, Mg/Al, and Fe/Al ratios (in molar if not specified) ranges of 0.12 – 0.57, 0.18 – 0.27, and 0.21 – 0.40, respectively (Table 2 and Figs. 2-3). Sample 164.90-2 (containing 10% calcite) exhibits the highest Ca/Al ratio (0.57), while sample 110.60-2 (containing siderite) shows the highest Mg/Al (0.27) and Fe/Al (0.40) ratios. In the leached residues, Ca/Al, Mg/Al, and Fe/Al ratios decrease systematically with increasing acid strength and concentration of the leaching reagents. Specifically, after treatment with 0.5 $mol \cdot L^{-1}$ HAc, 0.1 $mol \cdot L^{-1}$ HCl, and 0.4 $mol \cdot L^{-1}$ HCl, the Ca/Al ratios in the residues range from 0.0069 – 0.022, 0.0035 – 0.020, and 0.0023 – 0.020, respectively; Mg/Al ratios range from 0.16 – 0.25, 0.15 – 0.24, and 0.12 – 0.23; and Fe/Al ratios range from 0.21 – 0.39, 0.20 – 0.33, and 0.14 – 0.32. Accordingly, the leachate of each sample has Al/Ca, Mg/Ca and Fe/Ca ratios increasing with rising acid strength and concentration. Notably, the leachate of sample 110.60-2 displayed the highest Mg/Ca (0.37 – 1.2) and Fe/Ca ratios (0.40 – 1.9), consistent with the presence of Mg- and Fe-rich carbonate in this sample.

Five of the six diamictites exhibit whole rock $\delta^{26}Mg$ values (-0.020 ± 0.189‰, 2SD) higher than that of the mean upper continental crust (~ -0.22‰, [38] Fig. 4), as carbonates in these samples are dominantly calcium one (Table 3 and S2). Their leached residues via 0.5 $mol \cdot L^{-1}$ HAc, 0.1 $mol \cdot L^{-1}$ HCl and 0.4 $mol \cdot L^{-1}$ HCl all yielded $\delta^{26}Mg$ values deviating from whole rock data by no more than 0.074‰. Particularly, the leached residues of three diamictites have $\delta^{26}Mg$ values consistent with those of whole rock powders, irrespective of the leaching acid types and concentrations. Sample 110.60-2 that contains Mg- and Fe-rich carbonates also exhibits a low whole rock $\delta^{26}Mg$ of -0.454 ± 0.013‰; its residue $\delta^{26}Mg$ values show a systematic increase with acid strength (0.5 $mol \cdot L^{-1}$ HAc: -0.434 ± 0.010‰; 0.1 $mol \cdot L^{-1}$ HCl: -0.161 ± 0.022‰; 0.4 $mol \cdot L^{-1}$ HCl: 0.148 ± 0.018‰).

Efficiency of carbonate removal by different leaching methods. For most sediments, Al can be used as an indicator of the aluminosilicate component.[39] In the selective leaching experiments targeting carbonates, the solubility of Al is extremely low. Therefore, by comparing changes in the ratios of carbonate-related elements (e.g., Ca) to Al before and after leaching, the extent of carbonate mineral dissolution can be effectively evaluated. Compared to whole rock samples, Ca/Al ratios of their residue after treatment with 0.5 $mol \cdot L^{-1}$ HAc, 0.1 $mol \cdot L^{-1}$ HCl, and 0.4 $mol \cdot L^{-1}$ HCl exhibited substantial reductions of 81.2% – 97.4%, 82.7% – 98.9%, and 82.7% – 99.0%, respectively (Fig. 2a; Table 2). This finding indicates that both weak (0.5 $mol \cdot L^{-1}$ HAc) and strong acids (0.1 and 0.4 $mol \cdot L^{-1}$ HCl) were effective in calcite leaching. Except for sample 110.60-2, the leached residues of the other samples exhibited no systematic to minimal deviations in Mg/Al and Fe/Al ratios from whole rock values. This confirms the X-ray Diffraction (XRD) results that Mg- and Fe-poor calcite is the dominant carbonate phase in these samples (Table S2), and suggests that Mg and Fe dissolved from the silicate fractions were minimal at all the designed leaching conditions. By contrast, as shown by leaching experiments on sample 110.60-2, Mg- and Fe-rich carbonates can only be dissolved by strong acids like HCl (Figs. 2b and 2c; Figs. 3b and 3c; Table 2). The leaching of sample 110.60-2 with 0.5 $mol \cdot L^{-1}$ HAc resulted in only minor decreases of 7.7% and 1.4% in the Mg/Al and Fe/Al ratios of the residue compared to the whole-rock values. With increasing acid strength and concentration (i.e., leaching by 0.1 $mol \cdot L^{-1}$ HCl and 0.4 $mol \cdot L^{-1}$ HCl), the Mg/Al and Fe/Al ratios in residues decreased significantly, accompanied by markedly elevated Mg/Ca and Fe/Ca but moderately increased Al/Ca ratios in leachates. This systematic behavior indicates that significantly enhanced leaching of Mg and Fe from this sample under aggressive conditions resulted from the selective dissolution of acid-resistant Fe-Mg-rich carbonate minerals. Mineralogical (XRD)

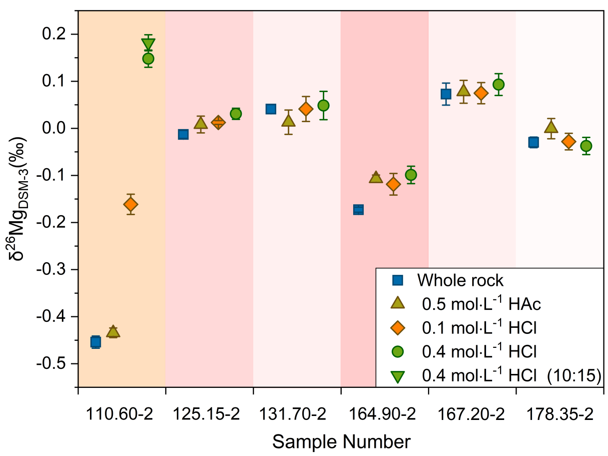

Fig. 5 Magnesium isotope composition of whole rock and leached residues of the selected diamictites. Blue squares represent the unleached whole-rock samples; while yellow-green triangles, orange diamonds, and green circles denote the residues from leaching 30 mg of sample with 10 mL of 0.5 mol·L^{-1} HAc, 0.1 mol·L^{-1} HCl, and 0.4 mol·L^{-1} HCl, respectively. The green inverted triangles indicate residues from leaching approximately 15 mg of sample with 10 mL of 0.4 mol·L^{-1} HCl. Different background colors are used to distinguish carbonate contents in the samples: light orange fields represent siderite-bearing samples; the gradient from light to dark red indicates increasing calcite content (1% – 10%) in the samples.

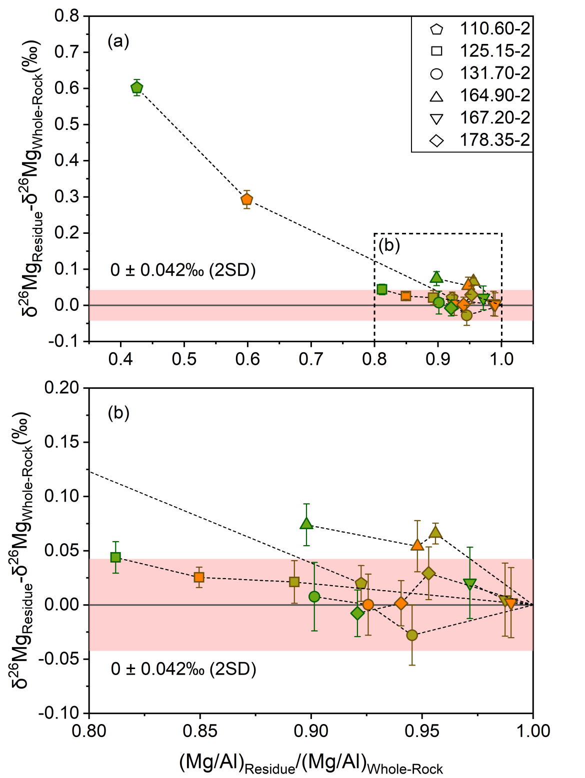

Fig. 6 Correlation between relative changes in Mg/Al ratios (Residue vs Whole rocks) and Mg isotopic offsets ($\delta^{26}Mg_{Residue}$ - $\delta^{26}Mg_{Whole\text{-}Rock}$). Different shapes correspond to different samples (see legend for identifiers), and colors represent the leaching treatments: yellow-green, orange, and green denote residues leached with 0.5 mol·L^{-1} HAc, 0.1 mol·L^{-1} HCl, and 0.4 mol·L^{-1} HCl, respectively. When whole-rock and residue Mg isotope values agree within analytical uncertainty, their difference ($\delta^{26}Mg_{Residue}$ - $\delta^{26}Mg_{Whole\text{-}Rock}$) should plot near the zero reference line in the figure. The pink band in the figure represents the ± 2SD range, propagated from the long-term analytical precision (~0.03‰ × √2).

and geochemical analysis of bulk-rock jointly corroborated this assumption. Sample 110.60-2 contains approximately 4% siderite (Table S2) and exhibits significantly higher whole rock Mg/Al and Fe/Al ratios (Table 2), distinguishing it from other samples.

Collectively, elemental data of leachates and residues reveal that HAc is adequate for calcite dissolution, while Fe- and Mg-rich carbonate components showcase limited solubility in 0.5 mol·L^{-1} HAc, and 0.4 mol·L^{-1} HCl is required for their sufficient dissolution. Our conclusion is supported by previous acid leaching experiments on Chinese loess, where weak HAc (0.1 or 0.5 mol·L^{-1}) and HCl (0.5 or 1.5 mol·L^{-1}) both achieve complete calcite dissolution, whereas only HCl dissolves most dolomite. [10]

Dissolution of silicate components during leaching. According to the results of mineralogical (XRD) analysis, Ca is primarily concentrated in carbonate minerals, making it a direct geochemical indicator for carbonates. Therefore, leachate Ca content can be used to as a reference to evaluate the carbonate composition and the dissolved silicate to carbonate ratio. The Al/Ca ratio was monitored as an indicator for unintended silicate leaching. [40] The Al/Ca ratios in leachates obtained with 0.5 mol·L^{-1} HAc, 0.1 mol·L^{-1} HCl, and 0.4 mol·L^{-1} HCl are all larger than 10%, significantly higher than any carbonate phases. These results demonstrate that silicate components undergo partial dissolution during leaching, regardless of whether strong or weak acids are employed. A 41 ± 14% (2SD, N = 6) increase in this ratio was observed when the leaching acid was replaced from 0.5 mol·L^{-1} HAc to 0.1 mol·L^{-1} HCl, and this ratio increased another 17 ± 10% (2SD, N = 6) when the concentration of the leaching HCl increased from 0.1 mol·L^{-1} to 0.4 mol·L^{-1}. A notable enhancement of silicate dissolution thus occurred under more aggressive leaching conditions (Fig. 3a; Table 2). This could also explain the increasing Mg/Ca and Fe/Ca with the acid intensity and concentration (Figs. 3b and 3c). The weakest silicate dissolution was observed in the leaching experiments using 0.5 mol·L^{-1} HAc, consistent with the documented capacity of low-concentration HAc to selectively extract carbonates with minimal damage to silicate matrices. [31] Conversely, HCl exhibited relatively poorer selective dissolution behavior, where a higher concentration directly led to increased silicate dissolution. [41]

Here we are particularly concerned with how Mg behaves during the leaching experiments. Magnesium in the silicate phase tends to be released concurrently with silicate dissolution. Given the low carbonate content (1% – 2%) and the presence of calcite as the only carbonate phase, samples 131.70-2, 167.20-2, and

Table 3. Mg isotopic data of whole rocks and leached residua of selected diamictites.

Sample No.	Mass	Reagent Volume	$\delta^{26}Mg_{DSM-3}$	2SE	n
	mg	mL	‰		
Whole Rocks					
110.60-2	3.97	–[a]	-0.454	0.013	4
125.15-2	4.93	–	-0.001	0.020	4
Replicate	4.40		-0.025	0.009	4
Mean	–	–	-0.013	0.009	8
131.70-2	4.87	–	0.045	0.010	4
Replicate	7.47		0.036	0.030	4
Mean	–	–	0.041	0.010	8
164.90-2	7.75	–	-0.169	0.006	4
Replicate	7.57		-0.177	0.016	4
Mean	–	–	-0.173	0.005	8
167.20-2	6.11	–	0.073	0.023	4
178.35-2	6.64	–	-0.030	0.011	4
Residue					
0.5 mol·L^{-1} HAc					
110.60-2	29.53	10	-0.434	0.010	4
125.15-2	30.80	10	0.008	0.018	4
131.70-2	29.58	10	0.013	0.026	4
164.90-2	29.19	10	-0.107	0.008	4
167.20-2	30.65	10	0.078	0.024	4
178.35-2	32.03	10	-0.001	0.022	4
0.1 mol·L^{-1} HCl					
110.60-2	32.85	10	-0.161	0.022	4
125.15-2	30.43	10	0.012	0.004	4
131.70-2	30.81	10	0.041	0.026	4
164.90-2	30.12	10	-0.119	0.023	4
167.20-2	30.71	10	0.075	0.022	4
178.35-2	30.38	10	-0.028	0.018	4
0.4 mol·L^{-1} HCl					
110.60-2	32.06	10	0.148	0.018	4
110.60-2*	16.10	10	0.182	0.017	4
125.15-2	29.52	10	0.031	0.012	4
131.70-2	31.90	10	0.049	0.030	4
164.90-2	31.31	10	-0.099	0.019	4
167.20-2	33.36	10	0.093	0.023	4
178.35-2	31.22	10	-0.037	0.018	4

Note: Replicate: independent repetitions of the complete experiment. Uncertainties are two standard errors of the mean, if not specified.
*: the experiment was performed with a reagent-to-solid ratio of approximately 10:15 (mL:mg). [a]: not given.

178.35-2 are suitable for assessing Mg mobilization resulting from silicate phase dissolution during leaching. After leaching with 0.5 mol·L^{-1} HAc, 0.1 mol·L^{-1} HCl, and 0.4 mol·L^{-1} HCl, the Mg/Al ratios in the residues of these three samples decreased by 1.3% – 5.5%, 1% – 7.4%, and 2.8% – 9.8%, respectively, relative to their whole-rock values. As 0.5 mol·L^{-1} HAc effectively removes calcite from the samples while inducing minimal alteration to silicate components, the Mg/Al ratios of the resulting residues can serve as a reference baseline for a scenario of least Mg release from the silicate phases. The Mg/Al ratios in the residues leached by 0.1 mol·L^{-1} HCl and 0.4 mol·L^{-1} HCl decreased by -0.3% to 2.1% and 1.6% to 4.7%, respectively, relative to the 0.5 mol·L^{-1} HAc-leached residues. These results demonstrate a general increasing trend in Mg loss from the silicate phase with rising acid strength and concentration. Nevertheless, the proportion of Mg released from the silicate phases remained limited (e.g., likely < 5%, and definitely < 10%) at the designed leaching conditions.

Mg isotope fractionation during the leaching process of glacial diamictite. As revealed by the elemental data, complete removal of Mg-rich carbonates from the diamictite powders requires leaching with strong acids of high concentrations, i.e., 0.4 mol·L^{-1} HCl here. Meanwhile, partial dissolution of the silicate phases is inevitable during leaching, and becomes more intensive with increasing acid strength and concentration. With the purpose to establish protocols for accurate δ^{26}Mg analysis of the silicate fractions of diamictites, it is crucial to evaluate i) whether δ^{26}Mg of the leached residue may be biased by isotope fractionation during partial dissolution of the silicate phases; and ii) whether Mg from the carbonate phase has been efficiently removed leaving insignificant contamination on the obtained leached residue.

The leached residues of samples 131.70-2, 167.20-2, and 178.35-2 that contain very trace calcite (1% – 2%; Table S2) by different leaching reagents yielded Mg isotopic compositions all consistent with their corresponding whole-rock values, with a mean $\delta^{26}Mg_{Residue}$ - $\delta^{26}Mg_{Whole-rock}$ value of 0.003 ± 0.032‰ (2SD, N = 9; Figs. 5 and 6; Table 3). Specifically, $\delta^{26}Mg_{Residue}$ - $\delta^{26}Mg_{Whole-rock}$ values for leaching treatments with 0.5 mol·L^{-1} HAc, 0.1 mol·L^{-1} HCl, and 0.4 mol·L^{-1} HCl were 0.002 ± 0.057‰ (2SD, N = 3), 0.001 ± 0.002‰ (2SD, N = 3), and 0.007 ± 0.028‰ (2SD, N = 3), respectively. It appears that $\delta^{26}Mg_{Residue}$ has not been significantly fractionated during the leaching experiments, despite that up to 10% Mg of the silicate phases was likely leached out at the severest conditions (Fig. 6). These observations confirm that carbonate is not a significant Mg carrier in these samples, given its much lighter isotopic composition relative to silicates (Fig. 4), and indicate that all three leaching protocols preserved the Mg isotopic integrity of the silicate fraction without significant fractionation.

The difference in Mg isotope values between the acid-leached residue and the whole rock was slight in sample 125.15-2 (~ 3% calcite; Table S2) but more pronounced in sample 164.90-2 (10% calcite; Table S2), corresponding to mean $\delta^{26}Mg_{Residue}$ - $\delta^{26}Mg_{Whole-rock}$ values of 0.030 ± 0.024‰ (2SD, N = 3) and 0.065 ± 0.020‰ (2SD, N = 3), respectively (Figs. 5 and 6; Table 3). In these two samples, the δ^{26}Mg values of the residues show no discernible difference among the three acid leaching methods within analytical uncertainty. It can be concluded that all three leaching acids effectively remove the light-Mg-enriched carbonate component, with 0.5 mol·L^{-1} HAc being sufficient for samples containing only calcite. And the consistent $\delta^{26}Mg_{Residue}$ across different acid treatments within analytical error confirms the insensitivity of the obtained silicate phase's isotopic composition to varying leaching conditions.

Significant differences were observed in the Mg isotope composition of the leaching residues from the siderite-bearing sample 110.60-2 after different leaching treatments. The δ^{26}Mg value of residue treated with 0.5 mol·L^{-1} HAc is identical within analytical uncertainty to that of the whole rock, yielding a $\delta^{26}Mg_{Residue}$ - $\delta^{26}Mg_{Whole-rock}$ difference of 0.020 ± 0.017‰ (2SE; Figs. 5 and 6; Table 3). The result is attributed to the selective dissolution of calcite (2 wt. %) in the sample by 0.5 mol·L^{-1} HAc, and it further validates that a low calcite content has a negligible impact on the whole-rock Mg isotope composition. However, the residues leached with 0.1 mol·L^{-1} HCl and 0.4 mol·L^{-1} HCl display elevated δ^{26}Mg values, corresponding to $\delta^{26}Mg_{Residue}$ - $\delta^{26}Mg_{Whole-rock}$ offsets of 0.293 ± 0.025‰ (2SE) and 0.602 ± 0.022‰ (2SE), respectively (Figs. 5 and 6; Table 3). Integrated elemental analyses demonstrate that Mg-Fe-rich carbonates exert significant control over the whole-rock Mg isotope composition. Removal of this component requires aggressive leaching conditions (0.4 mol·L^{-1} HCl), which effectively attacks the Mg-Fe-rich carbonates, with the Mg/Al ratio in the residue decreasing by 57.5% compared to the whole-rock value. Furthermore, leaching experiments on sample 110.60-2 at a higher reagent-to-solid ratio (10:15, mL:mg) showed that the $\delta^{26}Mg_{Residue}$ and Mg/Al obtained under this condition is consistent within analytical uncertainty with that acquired at the lower (10:30, mL:mg) reagent-to-solid ratio (Fig. 5, Tables 2 and 3). This further demonstrates that 0.4 mol·L^{-1} HCl achieves effective dissolution of Fe-Mg-rich carbonate components in the studied samples.

In summary, in samples with carbonate phases exclusively comprising ≤ 2% calcite, the trace Mg contribution from calcite causes negligible contamination in the silicate-phase Mg isotopic composition; with more calcite and/or the presence of Mg-rich carbonates, the Mg from the carbonate phase becomes significant and tends to bias the whole-rock δ^{26}Mg to lower values. For the later cases, leaching experiments are required to remove the carbonate phase for accurate Mg isotope analysis on the silicate fractions of diamictites.

Optimized one-step leaching protocol. Previous studies on carbonate-bearing sediments, HAc at different concentrations or dilute HCl has been widely utilized to achieve selective dissolution of carbonate phases. [11, 41-46] In studies targeting the silicate phase, some researchers have employed a two-step leaching procedure: the carbonate phases were first leached with an HAc solution, followed by treatment with HCl to remove any residual carbonate components. [15, 20] Conversely, other studies have utilized a direct HCl leaching method to remove carbonates. [47] Different acid reagents and leaching procedures are employed to extract or remove carbonate components from samples. However, the absence of unified standards and reference procedures prevents researchers from selecting the most appropriate acid reagent for leaching based on specific sample characteristics. Moreover, when these methods are applied to the study of Mg isotopes in silicate phases, the extent and variation in Mg isotopic fractionation of silicate components caused by different leaching methods remain unclear. Therefore, there is an urgent need to develop an optimized leaching method based on systematic evaluation—one that can effectively dissolve carbonates while minimizing the alteration of non-target phases and preventing artificial Mg isotope fractionation. Based on the experimental evidence from this study, we propose tailored one-step leaching protocols for silicate-phase Mg isotope analysis of glacial diamictite based on sample carbonate characteristics. For samples that only contain ≤ 2% calcite, no leaching pretreatment is necessary. For samples with more calcite, treatment with 0.5 mol·L^{-1} HAc for 30 minutes is recommended. For samples possessing complex carbonate assemblages such as Mg-Fe-rich carbonates, 0.4 mol·L^{-1} HCl should be utilized to achieve complete dissolution of all carbonate components, including the less soluble mineral phases. Although the experimental subjects of this study were limited to glacial diamictite samples, the applicability of this method can be further extended based on mineralogical analysis (XRD) results. Specifically, the leaching method proposed in this paper may also be applied to other sedimentary rocks with silicate mineral compositions similar to or simpler than those of the samples examined in this study.

CONCLUSION

The application of Mg isotopes (δ^{26}Mg) from silicate components as tracers of continental weathering history can be compromised by Mg contributed from primary carbonate phases. This interference requires the systematic pretreatment of samples prior to digestion. This study evaluated the leaching efficacy of three acid reagents (0.5 mol·L^{-1} HAc, 0.1 mol·L^{-1} HCl, and 0.4 mol·L^{-1} HCl). The results indicate that these acid treatments had negligible effects on the Mg isotope composition of the silicate fraction within the analytical uncertainty. Treatment with 0.5 mol·L^{-1} HAc at room temperature for 30 minutes effectively dissolved soluble calcite in the samples. For samples containing complex carbonate phases, such as Mg-Fe-rich carbonates, 0.4 mol·L^{-1} HCl is recommended as the optimal pretreatment reagent to achieve thorough extraction of carbonate phases while effectively preserving the original isotopic signature of the silicate fraction. Based on these findings, a leaching protocol for carbonate removal from detrital sedimentary rocks has been established. This protocol provides support for subsequent tracing of continental weathering using Mg isotopes.

ASSOCIATED CONTENT

The supporting information (Tables S1 – S5) is available at https://www.at-spectrosc.com.

AUTHOR INFORMATION

Yongsheng He is a Professor at the State Key Laboratory of Geological Processes and Mineral Resources, China University of Geosciences, Beijing (CUGB), leading a group focusing on Fe, Ca, and Mg isotope geochemistry. He received his B.S. (2005) and Ph.D. (2011) degrees in geochemistry from the University of Science and Technology of China. After completing his Ph.D., he came to CUGB for post-doctoral research and joined the Isotope Geochemistry Lab as a faculty in 2013. His main interest was petrogenesis of adakitic rocks and their implication on evolution of orogenic crust. He currently focuses on methodology developments on metal stable isotope geochemistry and its application in tracing key geological and planetary processes, e.g., deep carbon and oxygen cycles, changes in paleo-environment, and the formation and evolution of the Moon. He has published over 90 peer-reviewed scientific papers in ISI-indexed journals.

Shouming Chen is currently an Associate Research Professor at the Institute of Geology, Chinese Academy of Geological Sciences (CAGS). He received his BSc and MSc degrees from Jilin University in 2004 and 2007, respectively, and earned his PhD in 2010 from the CAGS. His long-term research interests include Neoproterozoic micropaleontology, chronostratigraphy, and paleoenvironmental studies. His current research focuses on the application of metal isotope systems to investigate the coupled evolution of the Neoproterozoic carbon cycle and atmosphere–ocean oxidation events (NOEs).

Corresponding Author

* Y. S. He

Email address: heys@cugb.edu.cn

* S. M. Chen

Email address: shoumingchen@foxmail.com

Notes

The authors declare no competing financial interest.

ACKNOWLEDGMENTS

This work was financially supported by the National Key Research and Development Project of China (2023YFF0804100), the National Natural Science Foundation of China (42288201, 42203063, and 42122019), Fundamental Research Funds for the Central Universities (2652023001), Hubei Provincial Key Research and Development Program (2024BCB098), and State Key Laboratory of Geological Processes and Mineral Resources.

REFERENCES

1. R. A. Berner and K. Caldeira, *Geology*, 1997, **25**, 955-956. https://doi.org/10.1130/0091-7613(1997)025<0955:TNFMBA>2.3.CO;2
2. L. R. Kump, S. L. Brantley, and M. A. Arthur, *Annu. Rev. Earth Planet. Sci.*, 2000, **28**, 611-667. https://doi.org/10.1146/annurev.earth.28.1.611
3. D. E. Penman, J. K. Caves Rugenstein, D. E. Ibarra, and M. J. Winnick, *Earth Sci. Rev.*, 2020, **209**, 103298. https://doi.org/10.1016/j.earscirev.2020.103298
4. A. S. Cohen, A. L. Coe, S. M. Harding, and L. Schwark, *Geology*, 2004, **32**, 157-160. https://doi.org/10.1130/g20158.1
5. J. Shen, R. Yin, S. Zhang, T. J. Algeo, D. J. Bottjer, J. Yu, G. Xu, D. Penman, Y. Wang, L. Li, X. Shi, N. J. Planavsky, Q. Feng, and S. Xie, *Nat. Commun.*, 2022, **13**, 299. https://doi.org/10.1038/s41467-022-27965-x
6. Z. Hu, S. Yang, C. Yang, Y. Guo, J. Xu, and C. Zhang, *Global Planet. Change*, 2023, **231**, 104307. https://doi.org/10.1016/j.gloplacha.2023.104307
7. T. M. Grygar, K. Mach, and M. Martinez, *Sediment. Geol.*, 2019, **382**, 75-84. https://doi.org/10.1016/j.sedgeo.2019.01.010
8. R.-H. Ye, F. Zhang, G.-Y. Wei, J. Chen, Z. Feng, and S.-Z. Shen, *Earth Planet. Sci. Lett.*, 2024, **647**, 119045. https://doi.org/10.1016/j.epsl.2024.119045
9. J. Shao, S. Yang, and C. Li, *Sediment. Geol.*, 2012, **265-266**, 110-120. https://doi.org/10.1016/j.sedgeo.2012.03.020
10. J. Yang, J. Chen, Z. An, G. Shields, X. Tao, H. Zhu, J. Ji, and Y. Chen, *Palaeogeogr. Palaeoclimatol. Palaeoecol.*, 2000, **157**, 151-159. https://doi.org/10.1016/S0031-0182(99)00159-5
11. P. A. E. Pogge von Strandmann, H. C. Jenkyns, and R. G.

Woodfine, *Nat. Geosci.*, 2013, **6**, 668-672. https://doi.org/10.1038/ngeo1875

12. J. Wimpenny, Q.-Z. Yin, D. Tollstrup, L.-W. Xie, and J. Sun, *Chem. Geol.*, 2014, **376**, 31-43. https://doi.org/10.1016/j.chemgeo.2014.03.008
13. F.-Z. Teng, *Rev. Mineral. Geochem.*, 2017, **82**, 219-287. https://doi.org/10.2138/rmg.2017.82.7
14. F.-Z. Teng, W.-Y. Li, R. L. Rudnick, and L. R. Gardner, *Earth Planet. Sci. Lett.*, 2010, **300**, 63-71. https://doi.org/10.1016/j.epsl.2010.09.036
15. K. J. Huang, F. Z. Teng, B. Shen, S. Xiao, X. Lang, H. R. Ma, Y. Fu, and Y. Peng, *Proc. Natl. Acad. Sci. U. S. A.*, 2016, **113**, 14904-14909. https://doi.org/10.1073/pnas.1607712113
16. X.-M. Liu, F.-Z. Teng, R. L. Rudnick, W. F. McDonough, and M. L. Cummings, *Geochim. Cosmochim. Acta*, 2014, **135**, 336-349. https://doi.org/10.1016/j.gca.2014.03.028
17. S.-J. Wang, F.-Z. Teng, R. L. Rudnick, and S.-G. Li, *Geochim. Cosmochim. Acta*, 2015, **165**, 435-448. https://doi.org/10.1016/j.gca.2015.06.019
18. X.-Y. Chen, F.-Z. Teng, K.-J. Huang, and T. J. Algeo, *Geochim. Cosmochim. Acta*, 2020, **287**, 263-276. https://doi.org/10.1016/j.gca.2020.02.035
19. J. Li, C. Hao, Z. Wang, L. Dong, Y. Wang, K.-J. Huang, X. Lang, T. Huang, H. Yuan, C. Zhou, and B. Shen, *Palaeogeogr. Palaeoclimatol. Palaeoecol.*, 2020, **552**, 109774. https://doi.org/10.1016/j.palaeo.2020.109774
20. G. Zhang, D. Chen, K.-J. Huang, M. Liu, T. Huang, R. Yeasmin, and Y. Fu, *Global Planet. Change*, 2021, **203**, 103518. https://doi.org/10.1016/j.gloplacha.2021.103518
21. C. Y. Liu, P. A. E. Pogge von Strandmann, G. Tarbuck, and D. J. Wilson, *Geostand. Geoanal. Res.*, 2022, **46**, 493-518. https://doi.org/10.1111/ggr.12441
22. E. E. Hiatt, P. K. Pufahl, and L. Guimarães da Silva, *Precambrian Res.*, 2020, **337**, 105533. https://doi.org/10.1016/j.precamres.2019.105533
23. Q.-R. Zhang, X.-L. Chu, and L.-J. Feng, Geological Society, London, Memoirs. London, Geological Society of London, 2011, **36**, 357-366. https://doi.org/10.1144/M36.32
24. C. Zhou, M. H. Huyskens, X. Lang, S. Xiao, and Q.-Z. Yin, *Geology*, 2019, **47**, 251-254. https://doi.org/10.1130/G45719.1
25. A. R. Tasistro-Hart, F. A. Macdonald, J. L. Crowley, and M. D. Schmitz, *Proc. Natl. Acad. Sci. U. S. A.*, 2025, **122**, e2418281122. https://doi.org/10.1073/pnas.2418281122
26. H. Bai, H. Kuang, Y. Liu, N. Peng, X. Chen, and Y. Wang, *Palaeogeogr. Palaeoclimatol. Palaeoecol.*, 2020, **559**, 109967. https://doi.org/10.1016/j.palaeo.2020.109967
27. P. Wang, Y. Du, W. Yu, T. J. Algeo, Q. Zhou, Y. Xu, L. Qi, L. Yuan, and W. Pan, *Earth Sci. Rev.*, 2020, **201**, 103032. https://doi.org/10.1016/j.earscirev.2019.103032
28. X. Lang, J. Chen, H. Cui, L. Man, K.-J. Huang, Y. Fu, C. Zhou, and B. Shen, *Precambrian Res.*, 2018, **310**, 243-255. https://doi.org/10.1016/j.precamres.2018.03.004
29. A. Tessier, P. G. C. Campbell, and M. Bisson, *Anal. Chem.*, 1979, **51**, 844-851. https://doi.org/10.1021/AC50043A017
30. Y. Liu, Y. Yang, Z. Yan, Z. Jin, C. Ye, P. A. E. Pogge von Strandmann, L. Deng, X. Liu, and X. Fang, *Global Planet. Change*, 2025, **253**, 104986. https://doi.org/10.1016/j.gloplacha.2025.104986
31. J. Lin, Y. Liu, Z. Hu, W. Chen, L. Zhang, and H. Chen, *Geostand. Geoanal. Res.*, 2019, **43**, 277-289. https://doi.org/10.1111/ggr.12260
32. S. Ke, F.-Z. Teng, S.-G. Li, T. Gao, S.-A. Liu, Y. He, and X. Mo, *Chem. Geol.*, 2016, **437**, 109-119. https://doi.org/10.1016/j.chemgeo.2016.05.002
33. R.-Y. Li, S. Ke, Y.-S. He, T. Gao, and X.-N. Meng, *Bull. Mineral., Petrol. Geochem.*, 2016, **35**, 441-447. https://doi.org/10.3969/j.issn.1007-2802.2016.03.005
34. Y. He, A.-Y. Sun, Y.-C. Zhang, R.-Y. Yang, S. Ke, Y. Wang, and F.-Z. Teng, *Solid Earth Sci.*, 2022, **7**, 188-199. https://doi.org/10.1016/j.sesci.2022.05.001
35. A. Galy, O. Yoffe, P. E. Janney, R. W. Williams, C. Cloquet, O. Alard, L. Halicz, M. Wadhwa, I. D. Hutcheon, E. Ramon, and J. Carignan, *J. Anal. At. Spectrom.*, 2003, **18**, 1352-1356. https://doi.org/10.1039/b309273a
36. X.-N. Liu, R. C. Hin, C. D. Coath, M. Bizimis, L. Su, D. A. Ionov, E. Takazawa, R. Brooker, and T. Elliott, *Geochim. Cosmochim. Acta*, 2023, **358**, 12-26. https://doi.org/10.1016/j.gca.2023.08.011
37. Y. Zhang, W. Yang, Y. Wang, Y. He, S. Ke, K. Qu, and S. Zhang, *Geostand. Geoanal. Res.*, 2025, **49,** 315-327. https://doi.org/10.1111/ggr.12598
38. W.-Y. Li, F.-Z. Teng, S. Ke, R. L. Rudnick, S. Gao, F.-Y. Wu, and B. W. Chappell, *Geochim. Cosmochim. Acta*, 2010, **74**, 6867-6884. https://doi.org/10.1016/j.gca.2010.08.030
39. N. Tribovillard, T. J. Algeo, T. Lyons, and A. Riboulleau, *Chem. Geol.*, 2006, **232**, 12-32. https://doi.org/10.1016/j.chemgeo.2006.02.012
40. P. A. E. Pogge von Strandmann, D. N. Schmidt, N. J. Planavsky, G. Wei, C. L. C. Jones, and K.-H. Baumann, *Chem. Geol.*, 2019, **530**, 119338. https://doi.org/10.1016/j.chemgeo.2019.119338
41. H. L. Taylor, I. J. K. Duivestein, J. Farkas, M. Dietzel, and A. Dosseto, *Clim. Past*, 2019, **15**, 635-646. https://doi.org/10.5194/cp-15-635-2019
42. J.-S. Ryu, N. Vigier, A. Decarreau, S.-W. Lee, K.-S. Lee, H. Song, and S. Petit, *Chem. Geol.*, 2016, **445**, 135-145. https://doi.org/10.1016/j.chemgeo.2016.02.006
43. A. D. Jacobson and J. D. Blum, *Geology*, 2000, **28**, 463-466. https://doi.org/10.1130/0091-7613(2000)28%3C463:SASGOD%3E2.0.CO;2
44. Y. Li, C. Li, Z. Chu, and J. Guo, *Microchem. J.*, 2021, **171**, 106880. https://doi.org/10.1016/j.microc.2021.106880
45. K.-J. Huang, B. Shen, X.-G. Lang, W.-B. Tang, Y. Peng, S. Ke, A. J. Kaufman, H.-R. Ma, and F.-B. Li, *Geochim. Cosmochim. Acta*, 2015, **164**, 333-351. https://doi.org/10.1016/j.gca.2015.05.002
46. J. G. Murphy, A.-S. C. Ahm, P. K. Swart, and J. A. Higgins, *Geochim. Cosmochim. Acta*, 2022, **337**, 140-154. https://doi.org/10.1016/j.gca.2022.09.019
47. Z. Jin, J. Yu, F. Zhang, and X. Qiang, *Quat. Sci. Rev.*, 2020, **248**, 106619. https://doi.org/10.1016/j.quascirev.2020.106619
48. M. X. Ling, F. Sedaghatpour, F. Z. Teng, P. D. Hays, J. Strauss, and W. Sun, *Rapid Commun. Mass Spectrom.*, 2011, **25**, 2828-2836. https://doi.org/10.1002/rcm.5172